Boundary-Layer Meteorol (2007) 125:1–24
DOI 10.1007/s10546-007-9190-9

ORIGINAL PAPER

Long-term study of coherent structures in the atmospheric surface layer

Christian Barthlott · Philippe Drobinski · Clément Fesquet · Thomas Dubos · Christophe Pietras

Received: 3 July 2006 / Accepted: 24 March 2007 / Published online: 7 July 2007
© Springer Science+Business Media B.V. 2007

Abstract A long-term study of coherent turbulence structures in the atmospheric surface layer has been carried out using 10 months of turbulence data taken on a 30-m tower under varying meteorological conditions. We use an objective detection technique based on wavelet transforms. The applied technique permits the isolation of the coherent structures from small-scale background fluctuations which is necessary for the development of dynamical models describing the evolution and properties of these phenomena. It was observed that coherent structures occupied 36% of the total time with mean turbulent flux contributions of 44% for momentum and 48% for heat. The calculation of a transport efficiency parameter indicates that coherent structures transport heat more efficiently than momentum. Furthermore, the transport efficiency increases with increasing contribution of the structures to the overall transport.

Keywords Atmospheric surface layer · Coherent structures · Microfront · Turbulence measurements · Wavelet analysis

C. Barthlott · C. Fesquet · T. Dubos · C. Pietras
Laboratoire de Météorologie Dynamique,
Institut Pierre Simon Laplace, École Polytechnique,
Palaiseau, France

C. Barthlott (✉)
Institut für Meteorologie und Klimaforschung,
Universität Karlsruhe/Forschungszentrum Karlsruhe,
POB 3640, 76021 Karlsruhe, Germany
e-mail: christian.barthlott@imk.fzk.de

P. Drobinski
Service d'Aéronomie, Institut Pierre Simon Laplace,
Université Pierre et Marie Curie,
Paris, France

1 Introduction

In recent years, coherent structures have been an important subject in atmospheric turbulence research from theoretical (e.g. Raupach et al. 1980, 1996), numerical (e.g. Su et al. 1998; Drobinski and Foster 2003; Drobinski et al. 2007; Foster et al. 2006) and experimental points of view (e.g. Gao et al. 1989; Paw U et al. 1992; Chen et al. 1997; Drobinski et al. 1998; Krusche and De Oliveira 2004; Drobinski et al. 2004). In the present work, the term coherent denotes a distinct, large-scale fluctuation pattern, which is regularly observed in a given turbulent flow. The large-scale structures organize and interact with smaller-scale fluctuations, but can retain their characteristic form (Wilczak 1984). Under convective conditions, the structures are evident in time traces of air temperature, vapour density, and other scalars, as ramp patterns in which a slow, nearly steady increase is followed by a relatively rapid change back to baseline level (Chen et al. 1997). Under stable conditions, two patterns are possible: (i) the pattern is inverted and a gradual fall is followed by a sudden rise or (ii) a sudden rise is followed by a gradual fall. In planetary boundary-layer turbulence, it is recognized that downdrafts (or sweeps) and updrafts (or ejections) are the primary constitutive motions of such coherent structures (Katul et al. 1997; Foster et al. 2006). Those ejection/sweep motions are usually associated with eddies generated and maintained by hydrodynamic instability associated with inflection points in the horizontal wind velocity profiles near the surface (Robinson 1991; Kanda and Hino 1993; McNaughton and Brunet 2002). The existence of humidity microfronts under neutral and stable stratification leads to the conclusion that the structures are not necessarily associated with buoyant convection (Gao et al. 1992; Paw U et al. 1992). In stable conditions, the picture of coherent structures is more complex due to the coexistence of turbulence and gravity waves. Lee et al. (1997) argue that nighttime waves and coherent motions belong to the same type of motion in the sense that both are generated by shear instability.

These coherent structures play an important role in momentum and scalar transport and their contribution to the turbulent fluxes must be accounted for in subgrid-scale parameterizations of mesoscale to global scale models (Foster and Brown 1994; Drobinski et al. 2006). However, particularly the coherent structure flux contribution covers a wide range of values in the open literature; e.g., Lu and Fitzjarrald (1994) find contributions of 37–45%, whereas in the study of Bergström and Högström (1989), even 90% of the transport is due to these phenomena. However, these high percentage values were observed only for short observation periods (1–2 h). Besides the complexity and natural variability of these structures, this large dispersion can mainly be attributed to the limitation on short data runs under particular meteorological conditions as well as the different detection and conditional sampling methods.

Despite the observational efforts during recent years, previous studies were limited by at least one of the following factors: first, data runs were limited to unstable conditions only. Secondly, only small datasets have been analyzed (Table 1) and finally, the determination of coherent structure duration and separation times was evaluated with relatively large uncertainties. Up to now, very few authors investigated longer datasets and a wider range of stability classes. Lu and Fitzjarrald (1994) examined a dataset covering 85 h for winter and summer cases including both convective and stable conditions with regard to the coupling between motions above and within a forest canopy. Brunet and Irvine (2000) used 350 h of data to investigate the streamwise spacing of the structures which was compared to theoretical predictions of Raupach et al. (1996). Recently, Thomas and Foken (2006) analyzed a large dataset with up to approximately 3,300 individual 30-min runs. However, after quality

Table 1 Comparison of dataset length and prevailing stratification of previous studies dealing with the experimental analysis of ramp-like coherent structures

Author	Dataset length	Stratification
Antonia and Chambers (1978)	1.5 h	Stable
Gao et al. (1989)	1.5 h	Unstable
Bergström and Högström (1989)	200 min	Unstable
Paw U et al. (1992)	Not noted	Unstable, neutral, stable
Gao et al. (1992)	23 h	Unstable, neutral, stable
Gao et al. (1993)	30 min	Unstable
Lu and Fitzjarrald (1994)	85 h	Unstable, stable
Qiu et al. (1995)	35 h	Unstable
Chen et al. (1997)	65 h	Unstable
Brunet and Irvine (2000)	350 h	Unstable, neutral, stable
Sadani and Kulkarni (2001)	2 days	Unstable
Krusche and De Oliveira (2004)	43 h	Unstable
Feigenwinter and Vogt (2005)	7 h (116 events)	Unstable
Thomas and Foken (2006)	Up to 1,650 h	Unstable, neutral, stable

control and partitioning of the data into three wind sectors, only 282–462.5 h of temperature fluctuation data remained for individual wind sectors.

The present paper addresses the above mentioned limitations by applying an objective and well-adapted methodology for coherent structure extraction. Our goal is to provide a picture of the process as completely as possible by using an extensive dataset including a wide range of atmospheric stability conditions. This enables us not only to give reliable mean values, but also to provide probability distributions of coherent structure statistics which show the range of possible values and also the most probable ones. Besides the frequency of occurrence, the mean and dominant time scales, the focus lies on the contribution of the structures to the overall turbulent transport. Especially, we want to answer the following questions: (i) How large is the contribution to the turbulent transport? (ii) Is the contribution dependent on meteorological parameters such as wind shear or stratification? (iii) How efficiently do the structures transport heat and momentum?

In Sect. 2, the measurements and data processing techniques as well as the detection method are described in detail. The results regarding the structural characteristics and energetics of coherent structures in the atmospheric surface layer are presented in Sect. 3. Section 4 concludes the study.

2 Measurements and data processing

2.1 Research site

The data used in this work were collected at the SIRTA observatory (http://www.sirta.fr) located at Palaiseau, 20 km south of Paris, France (Haeffelin et al. 2005). We use two CSAT sonic anemometers installed at 10 and 30 m heights (Campbell Scientific 2002). The tower is surrounded by different types of surface, i.e. close and distant forest, buildings and an open

Table 2 Atmospheric stability classes and Obukhov length L_*

Stratification	Range of L_* (m)
Unstable	$-1{,}000 < L_* \leq -200$
Very unstable	$-200 < L_* < 0$
Very stable	$0 \leq L_* < 200$
Stable	$200 \leq L_* < 1{,}000$
Neutral	$\lvert L_* \rvert \geq 1{,}000$

field sector (Fesquet et al. 2006). Since April 2005, consecutive turbulence measurements sampled with 10 Hz are available with only few interruptions due to system modifications. In the present study, we analyzed a ten month period from April 22 until August 25 and November 1, 2005 to April 30, 2006 which consists of 6,580 h of measurements. After quality control, the remaining dataset covers 5,721.5 h at 10 m and 6,088 h at 30 m height. In this study, we focus only on the open field sector (wind directions between 250 and 320°), where the fetch requirement is mostly fulfilled and the turbulence structure is less affected by surface heterogeneities than for the other wind directions. For this wind sector, the next obstacle is a small accumulation of trees about 1.6 km away and the estimated footprint for the flux measurements is smaller than the fetch distance to the next obstacles for westerly winds. The selection of this wind sector was confirmed by the smallest differences between the roughness lengths z_0 determined in both measuring heights indicating that both sonic anemometers are representing the same surface characteristics (Fesquet et al. 2006). Our first aim is to obtain a robust statistical analysis of the coherent structures for an adapted flow to a relatively smooth surface type. In a second work, Fesquet et al. (2006) analyze the effect of surface heterogeneity on the statistics of the coherent structures.

2.2 Data processing

We computed statistics of the measured data in 30-min blocks after rotating the coordinate system into the direction of the mean wind ($\overline{v} = \overline{w} = 0$) after Kaimal and Finnigan (1994). Since the lateral turbulent flux $\overline{v'w'}$ does not vanish completely after the coordinate rotation, the friction velocity u_* is calculated by

$$u_*^4 = \overline{u'w'}^2 + \overline{v'w'}^2, \tag{1}$$

where $\overline{u'w'}$ and $\overline{v'w'}$ are the turbulent fluxes in the longitudinal and lateral directions. As a measure of atmospheric stability, the Obukhov length L_* is defined as:

$$L_* = -\frac{u_*^3}{\kappa \frac{g}{\theta} \overline{w'\theta'}} \tag{2}$$

where κ is the von Karman constant, g is acceleration due to gravity and θ is potential temperature. The attribution of L_* to the atmospheric stability conditions is given in Table 2.

Before coherent motion detection, small-scale fluctuations are removed by digital filtering based on a fast Fourier transform whose cut-off frequency is 2 Hz. The cut-off frequency was chosen in such a way that, based on a cospectral analysis, the energy-containing range remains unaltered and only inactive high-frequent fluctuations are eliminated. This solely facilitates the structure detection by smoothing the time series. Since the large-scale variation of the signal is very slow, we additionally lower the sampling frequency to 1 Hz in order

to reduce computation time (see also Chen and Hu 2003). Furthermore, a linear trend was removed prior to coherent structure detection.

2.3 Ramp-signal detection with wavelet analysis

When dealing with coherent turbulence structures, a major difficulty is how to separate these organized features from background fluctuations (Chen and Hu 2003). Gao et al. (1989) and Bergström and Högström (1989) used turbulence time series measured at various levels to reconstruct the spatial patterns in time-height cross-sections. They found that a coherent structure involves a scalar microfront as a part of an ejection-sweep cycle of momentum. Afterwards, conditional sampling techniques like the VITA-method (Variable Interval Time Averaging; Schols 1984) or quadrant analysis (Wallace et al. 1972) became common tools for the investigation of these phenomena. As a first objective detection method, Collineau and Brunet (1993a) demonstrated the suitability of wavelet transforms for the detection of non-periodic signals with variable durations. The one-dimensional continuous wavelet transform of a function $x(t)$ with respect to an analyzing wavelet $\psi(t)$ is defined as:

$$W_n(s) = \frac{1}{s} \int_{-\infty}^{+\infty} x(t) \psi \left(\frac{t-n}{s} \right) \mathrm{d}t \tag{3}$$

where s is a scale dilation and n a position translation. A wavelet ψ is a real or complex valued function that must have zero mean. By varying the wavelet scale s and translating along the localized time index n, one can construct a picture showing both the amplitude of any patterns and how this amplitude varies with time (Torrence and Compo 1998). The choice of a wavelet is of particular importance, since the resulting correlation pattern will reflect the characteristics of the wavelet. The wavelet should possess a good localization in frequency space for the determination of characteristic scales, but should also be well localized in time space for event detection. Collineau and Brunet (1993a) compared four wavelets and demonstrated the advantages of the Mexican-Hat wavelet for jump detection. The Mexican-Hat wavelet is a compromise between a good frequency localization and a sufficient localization in time space. In addition, this wavelet reacts to the second derivative of the signal, which has a change in sign (a zero-crossing) at discontinuities such as ramps. Hence, this method avoids the uncertainty of empirically setting optimum detection thresholds, which is required for other wavelets (e.g., Haar, Ramp, Morlet). A number of authors have therefore used the Mexican-Hat wavelet and the zero-crossing of the wavelet coefficients to detect coherent structures in temperature time series (Chen et al. 1997; Brunet and Irvine 2000; Feigenwinter and Vogt 2005). In order to establish the most representative scale of the coherent structures, the global wavelet spectrum $\overline{W}(s)$ is computed as follows:

$$\overline{W}(s) = \int_{-\infty}^{\infty} |W_n(s)|^2 \mathrm{d}n. \tag{4}$$

According to Collineau and Brunet (1993a), the time scale associated with the maximum of $\overline{W}(s)$ corresponds to the mean duration of the most energetic turbulent structures.

Despite the efforts of investigating coherent turbulence structures in recent years, the definitions of their temporal boundaries are still not established (Krusche and De Oliveira 2004) which is key for deriving statistical properties like their duration or their contribution to the turbulent transport. Some authors such as Collineau and Brunet (1993b), Lu and Fitzjarrald (1994), Qiu et al. (1995) and Feigenwinter and Vogt (2005) included in their definition of the

coherent structures, portions of the temperature fluctuation time series that follow the sudden fall (i.e. microfront). Following the approach of Antonia et al. (1979), also applied by Paw U et al. (1992) or Krusche and De Oliveira (2004), the microfront determines the temporal/spatial end of the structure for convective conditions whereas it determines its beginning in the case of stable stratification where the pattern is inverted.

Figure 1 demonstrates the application of the wavelet transform to two time series with artificial ramp patterns. Under convective conditions, the end of the structure (the microfront) is represented by zero-crossings from positive to negative values whereas the beginning of the structure is represented by zero-crossings from negative to positive values for the case of stable stratification. The different slope sign for stable and unstable conditions is due to the different characteristics of the temperature ramps (unstable: gradual rise followed by sudden fall; stable: sudden rise followed by gradual fall). In order to derive parameters like duration, separation or contribution to the turbulent transport, the other boundary of the structure has to be specified. Some authors use a fixed time window around the zero-crossing of the wavelet coefficients (Feigenwinter and Vogt 2005) or the nearest zero-crossings in both directions of the microfront (Qiu et al. 1995). Gao et al. (1989) determines the length of a structure by taking into account the region with continuous updrafts preceeding the microfront to the region with continuous downdraft afterwards. The determination of the mean duration by the maximum of $\overline{W}(s)$ (applied by Gao and Li 1993; Lu and Fitzjarrald 1994) and the calculation of a mean separation by the number of zero-crossings only (applied by Brunet and Irvine 2000) can be influenced by the fact that the ramp patterns can have varying durations and separation times between ramps even inside an analyzed 30-min period (which is the block period chosen for this study). An improved approach is presented here where the graduation of the time series using the wavelet coefficients allows a dynamical adjustment to the varying scales as accurately as possible: starting from each microfront (detected by the zero-crossing of the wavelet coefficients), we use the preceeding minimum of the coefficients under convective conditions or the following one for stable situations to determine the duration D of each coherent structure separately (Figs. 1, 2). The remaining parts of the time series are the separation times S. Especially for the separation times, this method provides a more accurate result since long ramp-free periods and shorter separation times are detected as well. By doing this, we take into account the internal variability inside a 30-min period and have now the separation times between two detected structures which are not only calculated by the number of detections per data block. Another advantage is that the calculation of probability distributions can be based on all detected structures and not on half-hourly averaged duration or separation times.

Collineau and Brunet (1993a) pointed out that the zero-crossing method using the Mexican-Hat wavelet might identify too many structures during long ramp-free periods. For this reason, we introduce a threshold value for the detection: a coherent structure is identified only by those zero-crossings of the wavelet coefficients whose corresponding maximum (representing the amplitude of the ramp) exceeds at least 40% of the total maximum of the coefficients at the analyzed scale (Figs. 3, 4). The introduction of this selection criterion does not have to be considered as a constriction of the objectivity of our method, but rather a necessary supplementation when regarding long-term measurements which may include ramp-free periods. Another advantage of our method is the avoidance of overlapping structures which may have caused problems in the works of Lu and Fitzjarrald (1994) and Feigenwinter and Vogt (2005).

The individual steps of our detection method for a given temperature time series are as follows:

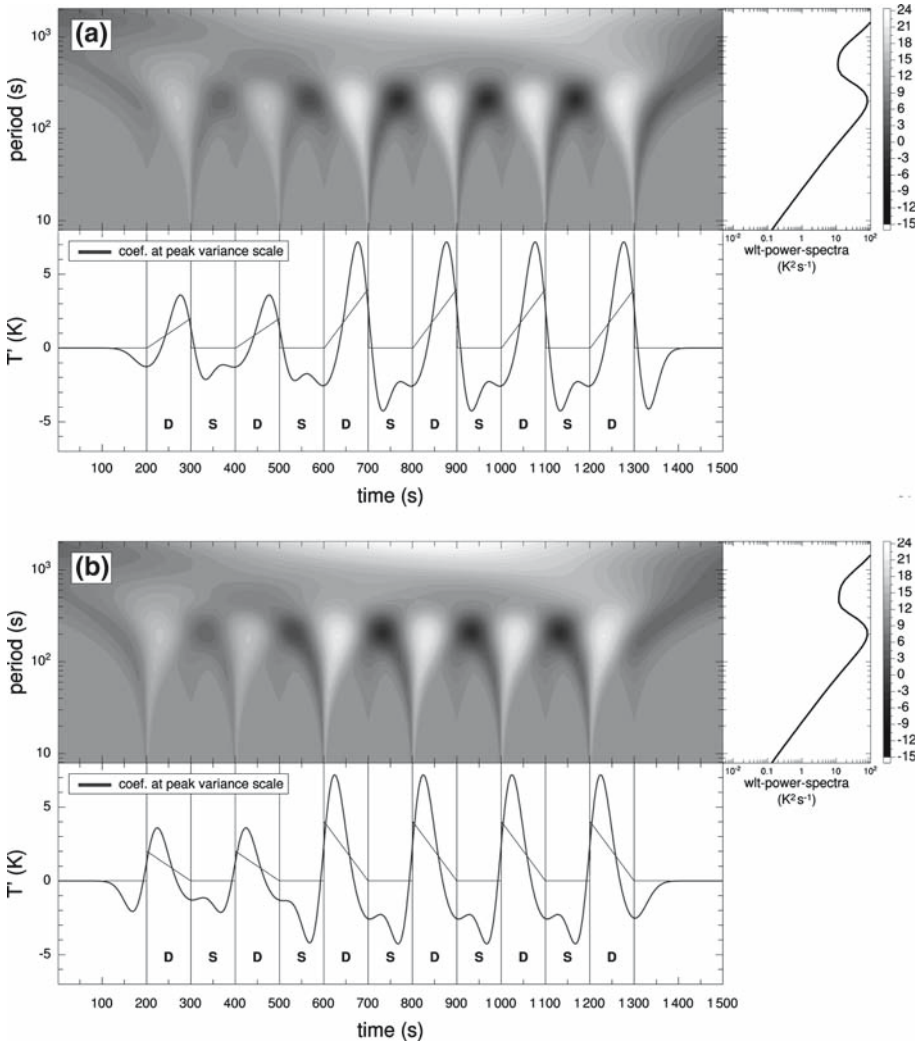

Fig. 1 Examples of the wavelet transformation for unstable (**a**) and stable conditions (**b**). Each sub-figure shows the wavelet coefficients $W_n(s)$ (*top*) of the artificial time-series (*bottom, black line*), the wavelet coefficients at the scale where the global wavelet spectrum has its maximum (*bottom, grey line*) and the global wavelet spectrum $\overline{W}(s)$ (*top right*)

1. remove small-scale fluctuations by digital filtering based on a fast Fourier transform (cut-off frequency 2 Hz);
2. lower the sampling frequency from 10 to 1 Hz and remove a linear trend;
3. calculate wavelet transforms for 30-min data runs and the global wavelet spectrum using the Mexican-Hat wavelet, and then
4. analyze the wavelet coefficients at the peak scale of the global wavelet spectrum depending on the type of stability

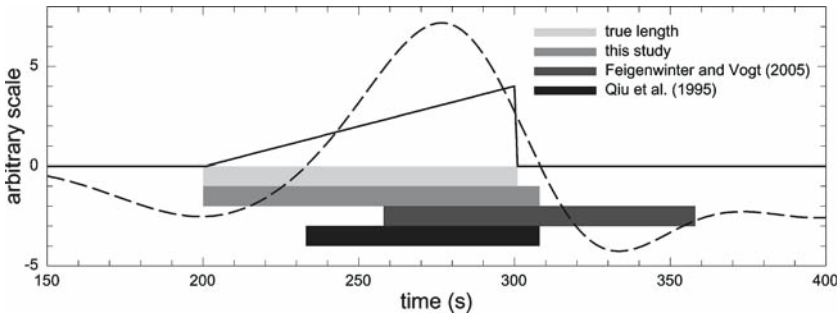

Fig. 2 Determination of the coherent structure duration of an artificial ramp pattern (*solid black line*) based on the wavelet coefficients at the maximum of $\overline{W}(s)$ (*dotted line*) for different methods

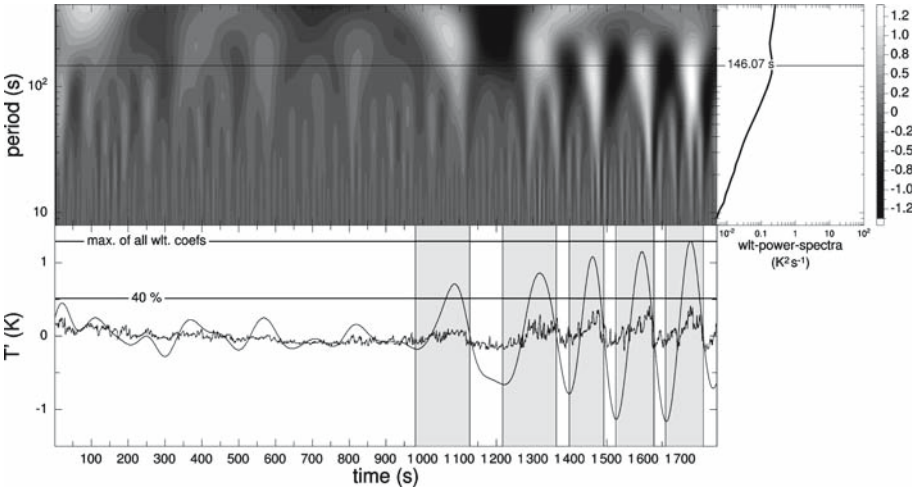

Fig. 3 As Fig. 1, but for temperature fluctuations of an unstable case on November 28, 2005 (1100–1130 UTC) at SIRTA observatory

- for unstable stratification:
  - determine the ending points of the structures by each zero-crossing of the wavelet coefficients with a negative slope whose preceeding local maximum exceeds a value of 0.4 times the absolute maximum of the coefficients at that scale, and
  - determine each starting point by the preceeding minimum of the wavelet coefficients.
- for stable stratification:
  - determine the starting points of the structures by each zero-crossing of the wavelet coefficients with a positive slope whose following local maximum exceeds a value of 0.4 times the absolute maximum of the coefficients at that scale, and
  - determine each ending point by the following minimum of the wavelet coefficients.

The results of this study are not influenced by steps 1 and 2, since they just smooth the time series and reduce the computation time. The large-scale signal remains unaltered. However, the choice of the threshold criteria has a strong impact on our results if long ramp-free periods

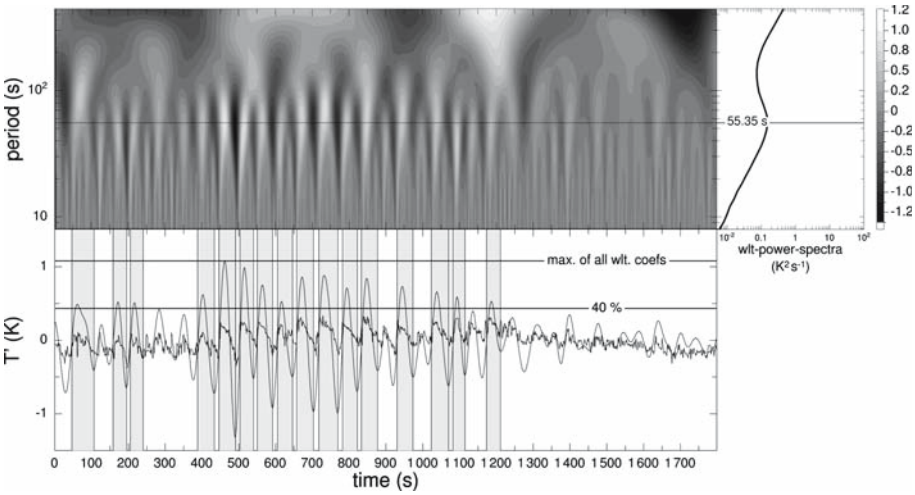

Fig. 4 As Fig. 1, but for temperature fluctuations of a stable case on May 31,2005 (2000–2030 UTC) at SIRTA observatory

exist. We tested a number of threshold values ranging from 20% to 60% for several days of measurements, the value of 40% seemed to be the most appropriate one. With this value, the bulk of the occurring structures was detected, structures on smaller scales were also detected and random-like fluctuations during ramp-free periods were discarded. In the range of 40%, the number of detected structures did not vary as much as in the range around 60% or 20%. However, false detections cannot be completely excluded, which is the reason why a visual inspection of all treated data-blocks was performed after the wavelet detection algorithm.

2.4 Coherent structure extraction examples from measurements

The examples in Figs. 3 and 4 demonstrate the applicability of our method, especially the introduction of the threshold value which prevents small-scale fluctuations to be detected as coherent structures during ramp-free periods. The grey shaded areas mark the results of our detection method. The starting and ending points of the ramp-patterns are matched satisfactorily both in unstable and stable conditions. However, the detected separation between individual ramps is slightly too large when consecutive ramps are present (Fig. 4). Another feature of Fig. 4 is the increase of energy towards longer periods after the local maximum located at 55 s due to the contribution from larger scales. This may occur when slow trends in the temperature signal are present, e.g. due to the presence of intermittent clouds (Collineau and Brunet 1993b). It is supposed that the first maximum starting from the high-frequency end of the variance spectrum is the most representative scale for the coherent structures. As an additional quality control, the global wavelet spectrum has to exhibit a well-defined peak at a reasonable scale in order to exclude inactive turbulence identified via large-scale peaks corresponding to trends in the data series. Furthermore, the mean wind speed has to exceed a value of 1 m s^{-1} in order to exclude data runs with low signal-to-noise ratio. In particular, this selection ensures the applicability of the eddy correlation technique under stable conditions, which becomes inappropriate if not enough turbulent activity exists (Caughey et al. 1979; Nieuwstadt 1984; Acevedo et al. 2006). Table 3 gives an overview of the data available after quality control, restriction to westerly winds and visual inspection of the wavelet detection

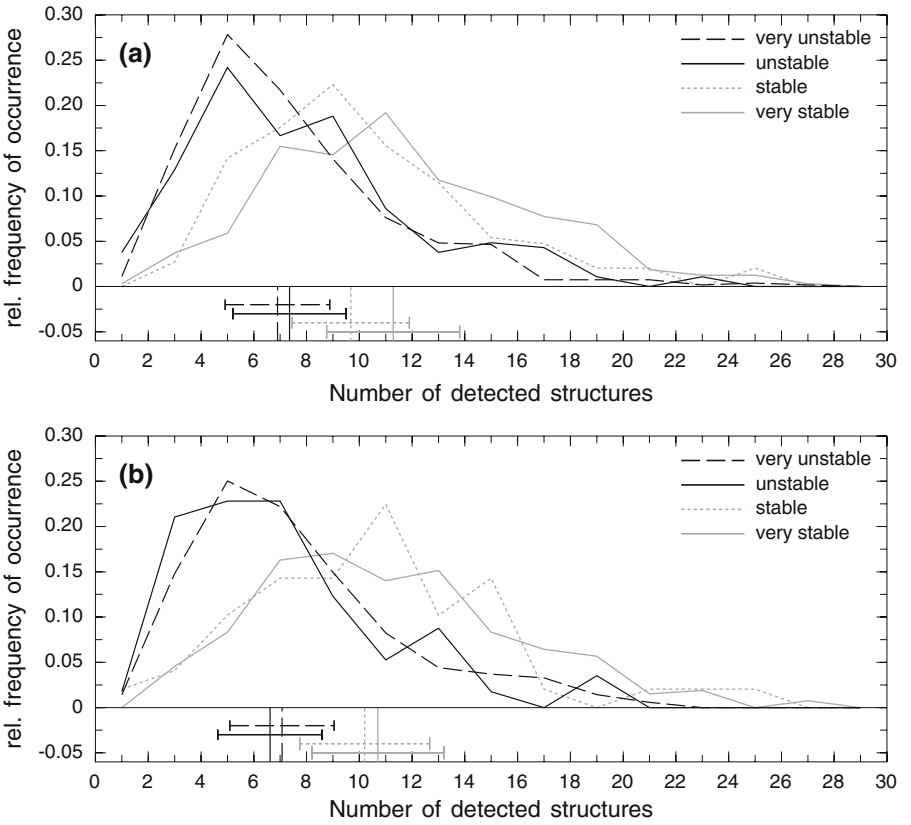

Fig. 5 Probability distribution of number of detected coherent structures at 30 m (**a**) and 10 m (**b**). The distribution of each stability class has been normalized with their number of occurrence, so that the sum of each probability equals 1. *Vertical straight lines* represent the respective mean value with errorbars

Table 3 Amount of available data for the different stability regimes after quality control, selection of westerly winds and good wavelet detection

	Stable	Very stable	Unstable	Very unstable	Total
10 m data (h)	24.5	132.5	28.5	351.5	537
30 m data (h)	74	162.5	93	269.5	599

method. The visual inspection was performed in order to avoid false detections during completely ramp-free periods. Due to the fact that temperature gradients disappear under neutral conditions, the detection of structures from temperature time series is almost impossible. However, the detection worked for a few selected events but due to their limited number, neutral conditions were discarded from the present statistical study.

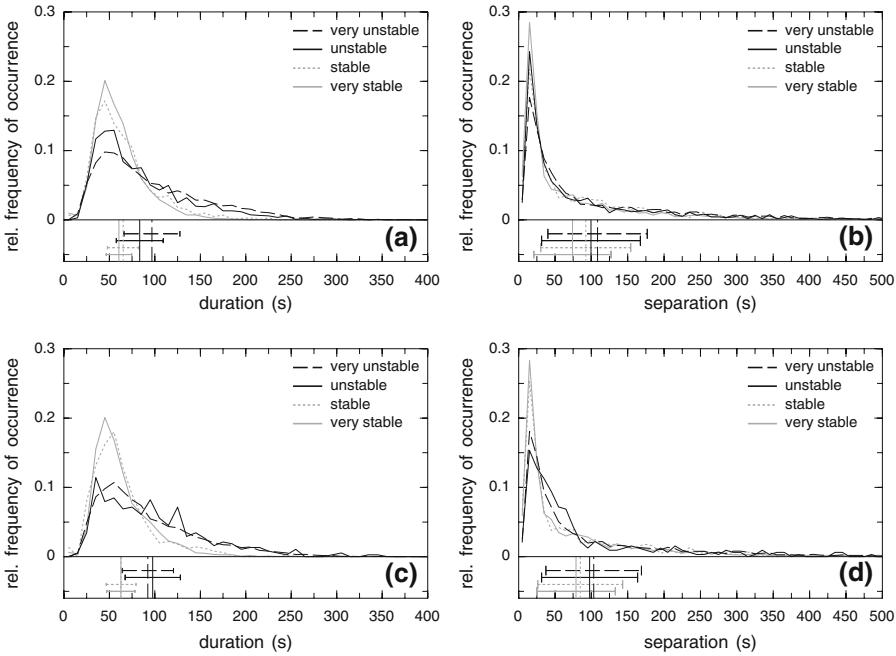

Fig. 6 Distribution of coherent structure duration and separation at 30 m (**a; b**) and 10 m (**c; d**). Same labelling as Fig. 5

2.5 Turbulence and internal gravity waves under stable stratification

The coexistence of turbulence and internal gravity waves in stable conditions may complicate the data analysis. Gravity waves and coherent structures have quite different properties and it is important to distinguish between them in order to avoid incorrect interpretation of the results. We performed spectral and cross-spectral analysis of a number of cases (i.e. 40) under stable conditions in order to separate the coherent structures from gravity waves, assuming the absence of non-linear interactions between them. When a wave is present, the spectra and cross-spectra of $\overline{w'T'}$ and $\overline{u'w'}$ should exhibit peaks associated with high levels of coherence and stable phase angles (Caughey and Readings 1975). For gravity waves, θ' is characteristically 90° out of phase with w' (Stull 1988), whereas for turbulence, the two variables are usually in phase for convection or 180° out of phase under stable conditions. In the frequency region of the coherent structures, the phase spectra clearly revealed that the variables are around 180° out of phase, which excludes the existence of linear gravity waves. This was found for all performed cross-spectral analysis.

Another possibility to investigate the presence of gravity waves is offered by the Brunt-Väisälä frequency N, which reflects the frequency of an oscillating parcel in stable conditions. It has been calculated on the basis of the 10 and 30 m temperature data as follows:

$$N^2 = \frac{g}{\theta_0}\frac{\partial\theta}{\partial z}, \tag{5}$$

with θ_0 being the mean potential temperature of both levels. It was observed that no correlation exists between the frequency of occurrence and N, which supports the conclusion that

Table 4 Mean and dominant values of coherent structure properties for the four stability classes

	Very stable		Stable		Unstable		Very unstable	
	Mean	Dom.	Mean	Dom.	Mean	Dom.	Mean	Dom.
FO_{10m} (30 min^{-1})	11	9	10	11	7	7	7	5
FO_{30m} (30 min^{-1})	11	11	10	9	7	5	7	5
D_{10m} (s)	63	45	63	55	98	35	92	55
D_{30m} (s)	61	45	65	45	83	55	97	45
S_{10m} (s)	79	15	85	15	98	15	103	15
S_{30m} (s)	74	15	92	15	100	15	109	15
L_{10m} (m)	170	75	301	175	558	775	407	225
L_{30m} (m)	236	175	378	225	593	375	468	225

our detection of turbulent coherent structures is not affected by the coexistence of turbulence and internal gravity waves under stable stratification.

3 Results

3.1 Structural characteristics

The statistical characteristics of coherent structures can be described by parameters like their frequency of occurrence FO, their duration D or separation time S. Using Taylor's hypothesis of frozen turbulence, the so-called Taylor length scale L is computed by multiplying the coherent structure duration time with the mean wind speed. In order to investigate the influence of atmospheric stratification, the probability distributions of those parameters have been calculated for each stability class (see Table 2) separately. The mean and dominant (most probable) values are listed in Table 4, whereas the probability distributions are displayed in Figs. 5–7.

As can be seen in Fig. 5, the number of coherent structures in the surface layer varies significantly. We observe on average between 7 and 11 structures every 30 min. There is no deterministic relationship between FO and the stability, which is in agreement with Gao et al. (1992). However, we do detect more structures under stable stratification than for convective conditions, but not of a sufficient nature to derive an analytical equation. Our values are comparable to other studies (e.g. Feigenwinter and Vogt 2005, 7–10 structures per 30 min). The probability distributions for the two stable regimes do not differ considerably nor do the two for the unstable ones. The differences of the mean values are explained by the different shapes of the distributions, which show a steeper increase with increasing number of structures and lower mean values for the unstable regimes.

As can be seen in Fig. 6, the distributions of the duration times show similar mean values for the two stable regimes (61–65 s). This is also observed for the two unstable regimes with mean values ranging between 83 and 98 s. Krusche and De Oliveira (2004) found values of 24–38 s for unstable stratification while Lu and Fitzjarrald (1994) found values of 52–54 s for unstable and stable stratification. According to our probability distributions (Fig. 6a, c), their values have a non-negligible probability of occurrence. Probably due to their limited datasets, they explore only a small portion of the range of possible values. In addition, differences of

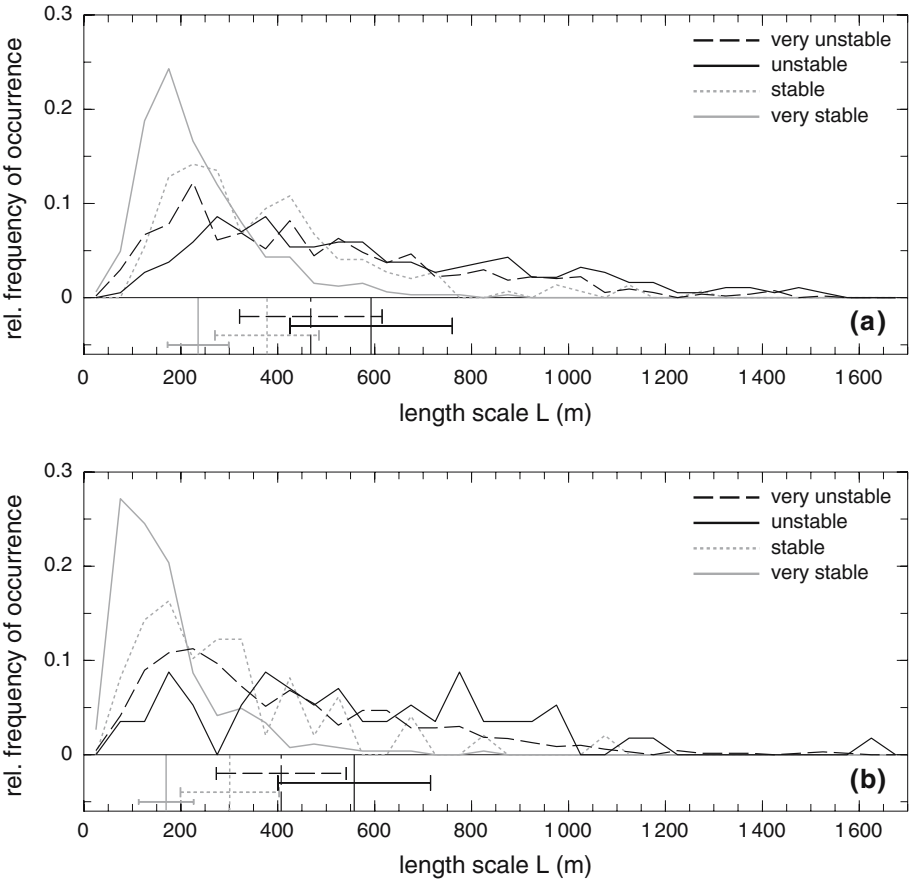

Fig. 7 Probability distribution of length scale L at 30 m (**a**) and 10 m (**b**). Same labelling as Fig. 5

the detection method or determination of duration times may also play a role, e.g., Krusche and De Oliveira (2004) evaluated the average coherent structure duration by taking only the first six intervals of the frequency distribution which automatically leads to smaller mean values. Since our detection method allows a dynamical adjustment on the varying scales of coherent structure duration and separation in each 30-min block, those time scales are determined more accurately. Using a large-eddy simulation, Su et al. (1998) find ramp structures with largest durations on the order of 130 s for unstable stratification, comparable to observations of Gao et al. (1989). The results of our long-term study are influenced by relatively rare large-scale structures which can develop under very convective conditions. Due to the low mean wind speed under these circumstances, the structures move very slowly and can therefore occupy long parts of the time series. In a recent work of Chen and Hu (2003), the coherent structure duration was determined from the maximum of the global wavelet spectrum for each velocity component, respectively. Average durations lie between 26 and 36 s for daytime conditions and 24–33 s for nighttime conditions, which leads the authors to the conclusion, that the main features of the structures at daytime and nighttime are almost the same.

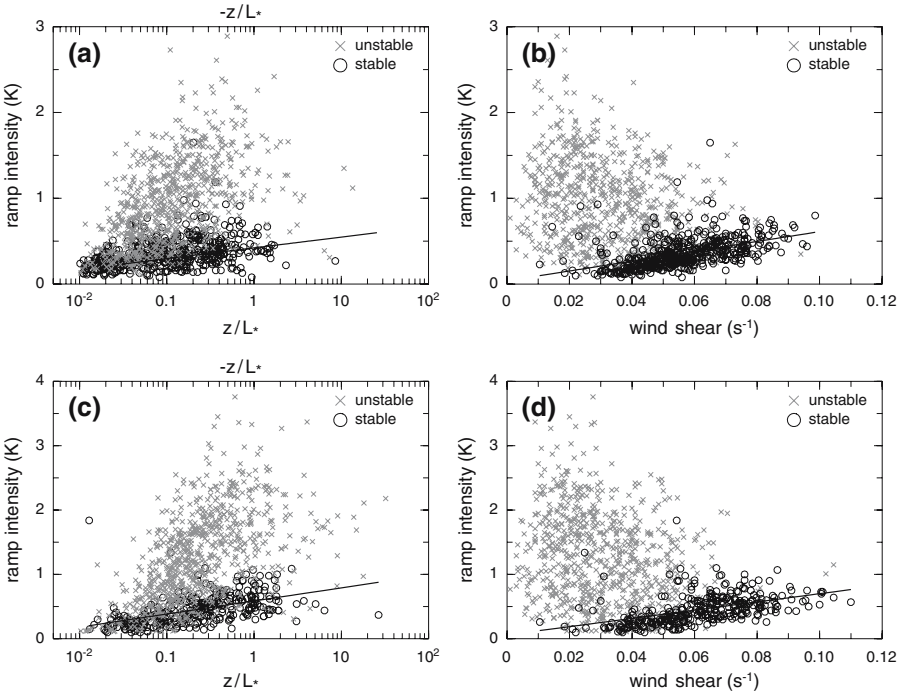

Fig. 8 Ramp intensity as a function of mean wind shear and stability parameter at 30 m (**a; b**) and 10 m (**c; d**)

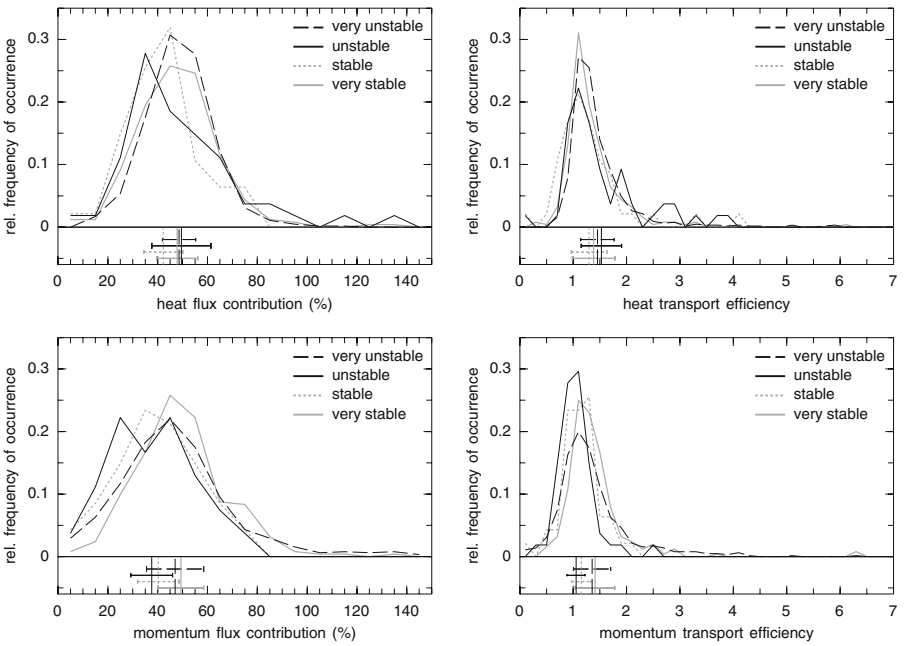

Fig. 9 Probability distributions of coherent structure flux contribution and transport efficiency at 10 m. The distributions of the flux contributions have been calculated in steps of 10%

As far as the most frequent duration times are concerned, the dominant values in this study lie between 35 and 55 s and no distinct dependence on the stratification is present. However, since the distribution of duration times is dependent on stratification, it can be divided into three sub-regions: (i) 1–30 s: structures with small durations occur at all stratifications with the same probability, (ii) 30–80 s: greater probabilities for structures under stable conditions and (iii) > 80 s: structures under convective conditions have larger probabilities. Due to the fact that we calculate the separation according to the temporal distance between individual ramp patterns (see Sect. 2.3), the mean separation times show large standard deviations. This reflects the fact that series of consecutive structures may occur as well as longer quiescent periods. Mean separation times only determined by the number of detected structures give certainly a more uniform picture, but also imply more errors when compared to our dynamical definition. Particularly, the consideration of ramp-free periods in our study yields the observed large standard deviations of the mean values. In the present study, the mean separation times between individual ramps increase with increasing instability in agreement with findings of Brunet and Irvine (2000) who found decreasing streamwise spacing with increasing stability. In their study, however, the number of all zero-crossings were counted to determine the average temporal separation. A reduced separation between adjacent structures in stable conditions may be related to the inhibition of turbulence, which does not allow the development of large structures (Brunet and Irvine 2000). A remarkable feature of the separation times is the independence of the dominant time scales (15 s) with respect to atmospheric stratification. As a consequence, the differences between the mean values are due to rare longer separation times under convective conditions only. Using a multi-level detection scheme, Gao et al. (1992) compute probability densities of the time interval between microfronts under stable conditions and finds averages of 84 s with a peak probability of 50 s. However, this time scale differs from our definition of the separation, which corresponds to the time interval between adjacent structures (i.e. the complete ejection/sweep cycle, Fig. 1). The time interval between microfronts does not include the length of the structure. As a consequence, the comparison with our results is not possible.

Concerning the associated length scales, we find a clear dependence of the mean Taylor length scale on the stratification, with structure sizes increasing with increasing instability (Fig. 7). However, we observe a reduction of the mean length scale for very unstable conditions, which is due to the reduction of the mean wind speed occurring at this type of stratification. The results of previous studies (Howell and Mahrt 1994: 100–600 m; Hagelberg and Gamage 1994: 500 m; Turner et al. 1994: 70–400 m) are part of our probability distributions, so the agreement with respect to these studies is reasonable. The higher mean length scales at the 30 m height are in agreement with the increasing eddy size with increasing distance from the ground. At the 10 m height, the probability distribution is irregular for unstable conditions due to the fact that only 28.5 h of data are available for this stratification class. The same applies for stable conditions (24.5 h). Another finding of Fig. 7 is the high probability of smaller-scale eddies under stable conditions as well as the increase of the standard deviation with increasing instability. This demonstrates the inhibition of large-scale structures under stable stratification. For convective conditions, however, there exists a much wider range of possible eddy sizes where the mean and dominant values become larger with increasing instability. The frequency of occurrence of coherent structures and their associated length scale are correlated in such a way that the length scale decreases with increasing number of structures (not shown).

Another important parameter for the statistics of turbulent coherent structures is their intensity. Therefore, the maximum ramp intensity of each 30-min block was extracted by using the maximum temperature value of the most intense ramp pattern. Under the absence

of non-linear trends, the baseline level to which the temperature jump usually returns lies at 0 K and the ramp intensity can therefore be determined solely from the maximum temperature value of the ramp after removal of a linear trend. Recent findings of Krusche and De Oliveira (2004) suggest that the ramp intensity is not related to characteristics of the surface-layer flow, such as the mean wind velocity, friction velocity, and stability parameter. In this study, however, we find a linear relationship between ramp intensity and wind shear for stable conditions (Fig. 8b, d) where the intensity increases with increasing wind shear. Under convective conditions, mean wind shear is smaller and no correlation can be observed. As far as the dependence on the stratification itself is concerned (Fig. 8a, c), the ramps become more intense with stronger stratification. Although there exists a large scatter for the unstable cases, this increase is still pronounced.

Besides the dependence on the stratification, no significant relationship between the coherent structure properties (frequency of occurrence, mean length, and time scales) and characteristics of the surface-layer flow (wind speed, wind shear, turbulent kinetic energy) was identified. Although the ramp intensity depends on stratification and wind shear, these findings raise the question whether it is possible to develop a parameterization of the contribution of the structures to the overall turbulent transport based on mean flow properties. Hence, we now focus on the energetical properties such as the coherent structure flux contribution and transport efficiency.

3.2 Contribution to total transport

The contribution of the coherent structures to the overall transport is of particular interest in boundary-layer research. However, the large variety of detection methods and conditional sampling procedures makes it difficult to compare the results of previous studies (Feigenwinter and Vogt 2005). Table 5 gives a short overview of studies dealing with coherent structure contribution to the turbulent transport based on measurements in the atmospheric boundary layer. It illustrates the differences of the results as well as the different datasets and applied methods. According to Lu and Fitzjarrald (1994), the contribution of the structures to total transport can be calculated as follows:

$$F_{\mathrm{coh}} = \left\{ \sum_{i=1}^{no} \overline{w'x'}_{\mathrm{coh}} \times t_{\mathrm{coh}} \right\} \Big/ \left(\overline{w'x'} \times t \right) \tag{6}$$

with:

$$\overline{w'x'}_{\mathrm{coh}} = t_{\mathrm{coh}}^{-1} \sum (w - \overline{w})(x - \overline{x}) \Big|_{\mathrm{coh}}, \tag{7}$$

$$\overline{w'x'} = t^{-1} \sum (w - \overline{w})(x - \overline{x}). \tag{8}$$

$\overline{w}$ and $\overline{x}$ are calculated over the entire half-hour period t, where x represents temperature T or the longitudinal velocity component u and no is the number of detected structures. $\overline{w'x'}_{\mathrm{coh}}$ is the conditional averaged flux of variable x for each coherent structure with duration t_{coh}. $\overline{w'x'}$ stands for the total Reynolds averaged turbulent flux. Due to the fact that a large time cover of the detected structures is supposed to provide a large contribution to the turbulent transport, it is mostly important not only to examine the flux contribution alone, but also to relate it to the net time cover TC of all detected structures. Therefore, we introduce a transport efficiency TE in order to relate the contribution of the structures to the fraction of time they occupy:

Table 5 Previous studies dealing with flux contributions of coherent structures

Study	Dataset	Surface	Detection method	F_{coh} $(\overline{u'w'})\%$	F_{coh} $(\overline{w'T'})\%$
Gao et al. (1989)	1.5 h	Deciduous forest	Visual detection	75	75
Bergström and Högström (1989)	200 min	Pine forest	Quadrant analysis	92.7	87.5
Collineau and Brunet (1993b)	4 h	Pine forest	Mexican-Hat wavelet (zero-crossing)	26	40
Howell and Mahrt (1994)	9.1 h	Flat terrain	Partitioning into 4 modes	50	–
Lu and Fitzjarrald (1994)	85 h	Deciduous forest	Haar wavelet	40	40
Hagelberg and Gamage (1994)	210 s	Aircraft data	Wavelet-based decomposition	–	64–74
Qiu et al. (1995)	35 h	Forest, orchard, maize field	Haar wavelet	–	50–80
Drobinski et al. (2004)	75 min	Flat terrain	Quadrant analysis	60	–
Feigenwinter and Vogt (2005)	7 h	Urban	Mexican-Hat wavelet (zero-crossing)	30–107	49–124

$$TE = \frac{F_{\text{coh}}}{TC} \tag{9}$$

with: (10)

$$TC = t^{-1} \sum_{i=1}^{no} t_{\text{coh}}. \tag{11}$$

TC represents the time cover of all detected structures inside a 30-min period in percent. Efficient (inefficient) processes have TE values greater (lower) than 1.

The probability distributions of coherent structure flux contribution for momentum and heat (Figs. 9, 10) reveal for some cases flux contributions greater than 100%, which seems to be nonsensical. However, detailed analysis of those cases revealed that they occurred during low turbulent activity when the overall transport is very weak. It can therefore be possible that the transport induced by the structures can be greater than the overall averaged transport and that quiescent periods surrounding the structures lead to a lower mean transport. One remarkable result of our investigation at SIRTA observatory is that coherent structures are, on average, not the dominant processes for the turbulent transport for most of the stability classes. As can be seen in Table 6, the mean values lie between 38–51% for momentum and 42–51% for heat. Only the flux contributions under very unstable conditions at 30 m are greater than 50%. All the results from Table 5 fit within the probability distribution, but the high flux contributions found by Gao et al. (1989) and Bergström and Högstrom (1989) are in the tail of the distribution. As far as the mean and dominant values are concerned, we observe no systematic dependence on the atmospheric stratification. The distributions are more Gaussian than the distributions for the time and length scales which is reflected by the relatively close mean and dominant values. It is also observed that coherent structures are very efficient for the turbulent transport with mean values of TE ranging from 1.05 to 1.66.

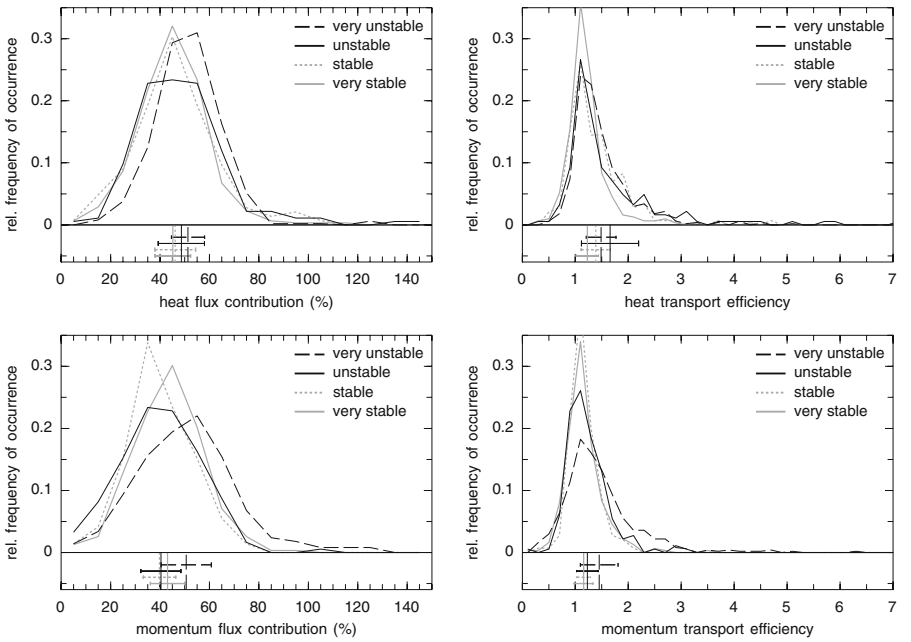

Fig. 10 Probability distributions of coherent structure flux contribution and transport efficiency at 30 m

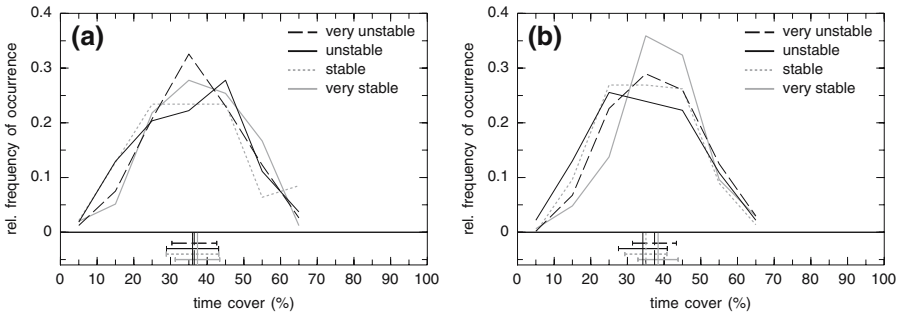

Fig. 11 Probability distributions of coherent structure time cover at 10 m (**a**) and 30 m (**b**)

Furthermore, all dominant values are greater than 1. Over 73% of all cases exhibit efficient transport properties for momentum whereas even over 85% are efficient for heat transport. Another finding of Figs. 9, 10 and Table 6 is the higher contribution of the structures to the sensible heat flux compared to momentum flux. As a consequence, the structures do transport heat more efficiently than momentum. Furthermore, on average 34–38% of the analyzed dataset is covered by coherent structures (Fig. 11). We also observe an upper limit for the time coverage of 70% and no systematic dependence on stratification. We therefore can conclude that the reduced number of coherent structures under convective conditions is just balanced by their larger duration times in such a way that the mean time cover stays the same.

Table 6 Mean and dominant values of flux contribution, time cover and transport efficiency for the four stability classes

	Very stable		Stable		Unstable		Very unstable	
	Mean	Dom.	Mean	Dom.	Mean	Dom.	Mean	Dom.
$F_{\mathrm{coh}}(uw)_{10\mathrm{m}}$ (%)	49	45	40	35	38	45	47	45
$F_{\mathrm{coh}}(wT)_{10\mathrm{m}}$ (%)	48	45	42	45	50	35	49	45
$TE(uw)_{10\mathrm{m}}$	1.41	1.1	1.15	1.3	1.05	1.1	1.35	1.1
$TE(wT)_{10\mathrm{m}}$	1.38	1.1	1.30	1.1	1.53	1.1	1.45	1.1
$TC_{10\mathrm{m}}$ (%)	37	35	36	45	36	45	36	35
$F_{\mathrm{coh}}(uw)_{30\mathrm{m}}$ (%)	43	45	40	35	40	35	51	55
$F_{\mathrm{coh}}(wT)_{30\mathrm{m}}$ (%)	45	45	46	45	49	45	51	55
$TE(uw)_{30\mathrm{m}}$	1.16	1.1	1.16	1.1	1.23	1.1	1.45	1.1
$TE(wT)_{30\mathrm{m}}$	1.23	1.1	1.39	1.1	1.66	1.1	1.49	1.1
$TC_{30\mathrm{m}}$ (%)	38	35	35	35	34	25	37	35

3.2.1 Dependence of flux contribution on coherent structure properties

Due to the fact that we observe no relationship between the flux contribution and other flow parameters, such as the mean wind speed, wind shear, or turbulence intensity, it is now of special interest to investigate its dependence on coherent structure properties. Our results show that the flux contribution is not dependent on the number of coherent structures. We only observe an increase of flux contribution in the range of 1–4 detected structures, whereas it becomes totally independent from the number of structures for 5 or more detections (not shown). We do observe, however, an increasing flux contribution with increasing time cover (Fig. 12). The fact that a large time cover is related to a large flux contribution is not surprising, but the observed linear relationship is remarkable. If we consider only those data points where the respective turbulent flux reaches at least 25% of the total maximum flux, the scatter reflecting the large variability of the process becomes much weaker. Another finding of Fig. 12 is the steeper slope for momentum (10 m: 0.87; 30 m: 0.80) compared to heat flux contribution (10 m: 0.65, 30 m: 0.57). This indicates that momentum flux contribution increases more than heat flux contribution with increasing time cover. Due to the large scatter, the interpretation is delicate. However, it is significant that the flux contribution depends on the time cover of all detected structures and not on the number of detections itself.

As far as transport efficiency is concerned, no dependencies with flow parameters were found. We therefore investigate the behaviour of the transport efficiency with respect to the flux contribution. Figure 13 displays the fraction of transport efficiencies greater and lower than 1 as a function of flux contribution in steps of 10%. Towards higher flux contributions, we observe an increasing percentage of efficient transport processes indicating more efficient transports for large flux contributions. Furthermore, all transport processes are efficient at both measuring heights independent of the transported parameter for contributions greater than 70%. The threshold at which efficient transport processes become dominant (probabilities $> 50\%$) increases with the measuring height for heat and momentum flux contributions. This could emphasize the importance of wind shear for the generation and dynamics of coherent structures since the wind shear increases with decreasing height. In addition, the transport efficiency does not depend on the number of detected structures (not shown). Our

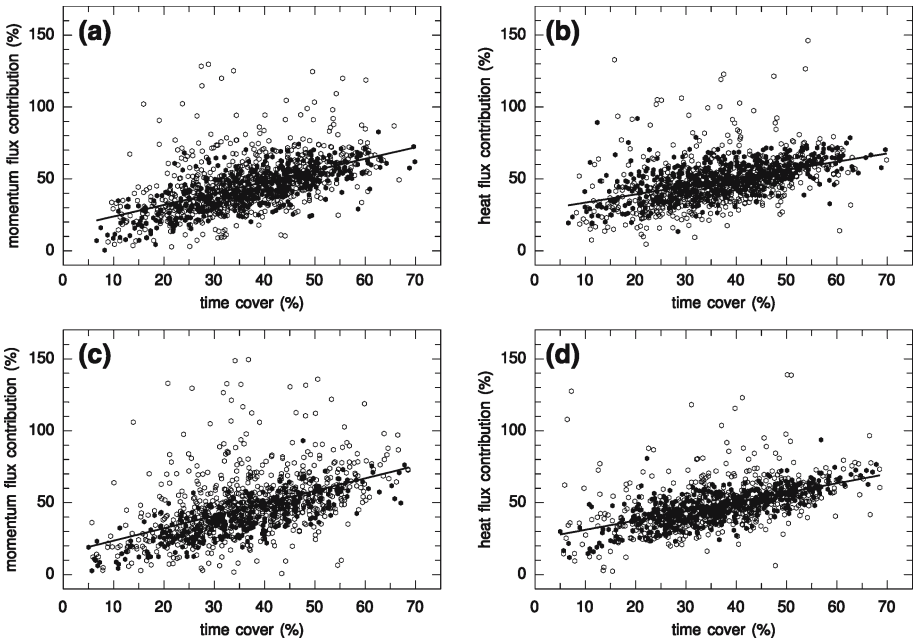

Fig. 12 Variation of coherent structure flux contribution with time cover at 30 m (**a; b**) and 10 m (**c; d**). *Filled dots*: for fluxes greater than 25% of maximum value, *open dots*: fluxes lower than 25% of maximum value

findings suggest that large contributions of the coherent structures to the overall transport are not only realized by a large time cover, but are also a consequence of more efficient transport.

4 Conclusions

In this work, a long-term study of the occurrence and properties of turbulent coherent structures in the atmospheric surface layer was performed. Our main contribution lies in methodical enhancements (dynamical determination of coherent structure duration, identification of separation times between adjacent structures, accounting for ramp-free periods) and the large amount of data used for the study. It enables us, not only to compute mean values, but also to deliver probability distributions of coherent structure properties (duration, separation, flux contribution) which show the range of possible values and also the most probable ones for different meteorological conditions.

Our results show that coherent structures occur more often under stable conditions than for unstable conditions but with smaller length scales. The almost vanishing dependence of the time cover on atmospheric stability leads us to the conclusion that the lower frequency of occurrence under convective conditions is balanced by longer persisting structures in such a way that the mean time cover remains unaltered. The duration and separation times of the structures are highly variable in the surface layer but a well pronounced peak in the probability distributions indicates that the dominant separation times do not depend on atmospheric stratification. We could therefore expand the findings of Gao et al. (1992) and Raupach et al. (1996) to smooth surfaces, who state that coherent temperature structures are dynamically linked to the wind shear and that they are not necessarily associated with buoyant convection.

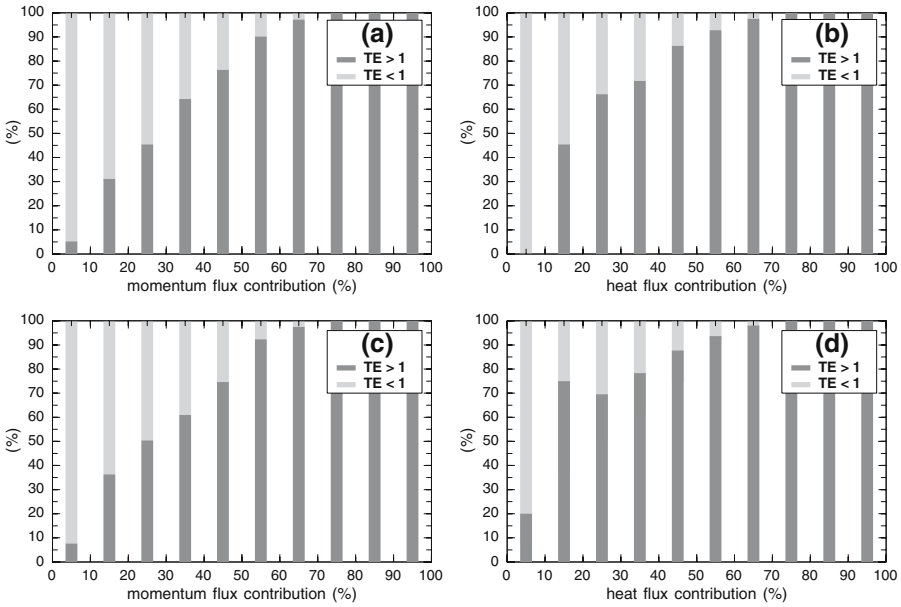

Fig. 13 Variation of transport efficiency with flux contribution at 30 m (**a; b**) and 10 m (**c; d**)

However, the stability dependence of the frequency of occurrence or the duration times still emphasize the role of stratification for the formation of coherent eddies. Furthermore, the increase of the ramp intensity with stronger stratification also supports this finding. This result is in agreement with recent findings of Thomas and Foken (2006), who state that under unstable stratification, organized motion is a superposition of shear driven and thermal structures.

The structures occupy 36% of the total time with mean contributions of 44% for momentum and 48% for heat. Our long-term study reveals that for some cases, coherent structures are the dominant processes for the turbulent transport and during others they are not. For a given stability class, it is now possible to specify the most probable of the associated flux contributions. Our results are in agreement with Lu and Fitzjarrald (1994), who state that coherent structures are not necessarily more important than other motions for determining fluxes. It is also shown that the flux contribution does not depend on the number of detected structures but increases linearly with increasing overall time cover. Furthermore, the calculation of a transport efficiency parameter indicates that the bulk of the associated transport is efficient and that coherent structures transport heat more efficiently than momentum. This fact can also be influenced by the vertical gradients of wind speed and temperature or different momentum and thermal diffusivities. We have also investigated the relationship between the ratio of the two flux contributions regarding the Prandtl number (ratio of momentum to thermal diffusivity) and, unfortunately, none was identified. One must note, however, that the use of a "bulk" Prandtl number for which the vertical gradients of temperature and wind speed are calculated using finite differences between 10 and 30 m is accurate for stably to unstably stratified boundary layers but can lead to large errors in the very stable boundary layer as discussed in Poulos and Burns (2003) and Drobinski et al. (2006). Furthermore, the transport efficiency increases with increasing contribution of the structures to the overall transport which leads us to the conclusion that large flux contributions are created by a large time cover and more efficient transport processes as well.

Due to the wide range of detection and conditional sampling techniques, further investigations must be made in order to determine the influence of the applied methods on the results. An intercomparison of several methods on the same dataset would allow an intercomparison between the different concepts. Furthermore, there still remains the question whether the results are also site-dependent since the underlying surface ranges from open land, over forests to urban areas. Fesquet et al. (to be submitted) go further into this question by investigating the occurrence of coherent structures as a function of different wind sectors (open land, near and distant forest, buildings) at the SIRTA observatory using the same data base and coherent structure analysis technique.

Acknowledgements We would like to thank the Centre National de la Recherche Scientifique (CNRS), the Direction Générale de l'Armement (DGA) and the École Polytechnique, Palaiseau, for funding Ch. Barthlott's visit at LMD. This research has also been funded by the Institut des Sciences de l'Univers (INSU) through the Programme Atmosphère Océan à Multi-échelle (PATOM). We are also grateful to the SIRTA scientific director M. Haeffelin and the SIRTA team. Wavelet software was provided by C. Torrence and G. Compo, and is available at URL: `http://paos.colorado.edu/research/wavelets/`.

References

Acevedo OC, Moraes OLL, Degrazia GA, Medeiros LE (2006) Intermittency and the exchange of scalars in the nocturnal surface layer. Boundary-Layer Meteorol 119:41–55

Antonia RA, Chambers AJ (1978) Note on the temperature ramp structure in the marine surface layer. Boundary-Layer Meteorol 15:3347–3355

Antonia RA, Chambers AJ, Friehe CA, Van Atta CW (1979) Temperature ramps in the atmospheric surface layer. J Atmos Sci 36:99–108

Bergström H, Högström U (1989) Turbulent exchange above a pine forest, II: organized structures. Boundary-Layer Meteorol 49:231–263

Brunet Y, Irvine MR (2000) The control of coherent eddies in vegetation canopies: streamwise structure spacing, canopy shear scale and atmospheric stability. Boundary-Layer Meteorol 94:139–163

Campbell Scientific (2002) CSAT Three dimensional sonic anemometer – User guide, Issued 04.9.02. Campbell Park, Shepshed, Loughborough, UK, 38 pp

Caughey SJ, Readings CJ (1975) An observation of waves and turbulence in the earth's boundary layer. Boundary-Layer Meteorol 9:279–296

Caughey SJ, Wyngaard JC, Kaimal JC (1979) Turbulence in the evolving stable boundary layer. J Atmos Sci 36:1041–1052

Chen J, Hu F (2003) Coherent structures detected in atmospheric boundary-layer turbulence using wavelet transforms at Huaihe river basin, China. Boundary-Layer Meteorol 107:429–444

Chen W, Novak MD, Black TA, Lee X (1997) Coherent eddies and temperature structure functions for three contrasting surfaces. Part I: Ramp model with finite microfront time. Boundary-Layer Meteorol 84:99–123

Collineau S, Brunet Y (1993a) Detection of turbulent coherent motions in a forest canopy, Part 1: wavelet analysis. Boundary-Layer Meteorol 65:357–379

Collineau S, Brunet Y (1993b) Detection of turbulent coherent motions in a forest canopy, Part 2: time-scales and conditional averages. Boundary-Layer Meteorol 66:49–73

Drobinski P, Foster RC (2003) On the origin of near-surface streaks in the neutrally-stratified planetary boundary layer. Boundary-Layer Meteorol 108:247–256

Drobinski P, Brown RA, Flamant PH, Pelon J (1998) Evidence of organized large eddies by ground-based Doppler lidar, sonic anemometer and sodar. Boundary-Layer Meteorol 88:343–361

Drobinski P, Carlotti P, Newsom RK, Banta RM, Foster RC, Redelsberger J-L (2004) The structure of the near-neutral atmospheric surface layer. J Atmos Sci 61:699–714

Drobinski P, Carlotti P, Redelsberger J-L, Banta RM, Masson V, Newsom RK (2007) Numerical and experimental investigation of the neutral atmospheric surface layer. J Atmos Sci 64:137–156

Drobinski P, Redelsberger J-L, Pietras C (2006) Evaluation of a planetary boundary layer subgrid-scale model that accounts for near-surface turbulence anisotropy. Geophys Res Lett 33: L23806. doi:10.1029/2006GL027062

Feigenwinter C, Vogt R (2005) Detection and analysis of coherent structures in urban turbulence. Theor Appl Climatol 81:219–230

Fesquet C, Barthlott C, Drobinski P, Dubos T, Pietras C, Haeffelin M (2006) Impact of terrain heterogeneity on near-surface turbulence: long-term investigation at SIRTA observatory. In: 17th Symposium on Boundary Layers and Turbulence/27th Conference on Agricultural and Forest Meteorology, AMS paper no. J6.6, San Diego, USA

Foster RC, Brown RA (1994) On large-scale PBL modelling: surface layer models. Global Atmos Ocean Syst 2:185–198

Foster RC, Vianey F, Drobinski P, Carlotti P (2006) Near-surface coherent structures and the vertical momentum flux in a large-eddy simulation of the neutrally-stratified boundary layer. Boundary-Layer Meteorol 120:229–255

Gao W, Li BL (1993) Wavelet analysis of coherent structures at the atmosphere-forest interface. J Appl Meteorol 32:1717–1725

Gao W, Shaw RH, Paw U KT (1989) Observation of organized structure in turblent flow within and above a forest canopy, Boundary-Layer Meteorol 47:349–377

Gao W, Shaw RH, Paw U KT (1992) Conditional analysis of temperature and humidity microfronts and ejection/sweep motions within and above a deciduous forest. Boundary-Layer Meteorol 59:35–57

Haeffelin M, Barthès L, Bock O, Boitel C, Bony S, Bouniol D, Chepfer H, Chiriaco M, Delanoë J, Drobinski P, Dufresne JL, Flamant C, Grall M, Hodzic A, Hourdin F, Lapouge F, Lemaître Y, Mathieu A, Morille Y, Naud C, Noël V, Pelon J, Pietras C, Protat A, Romand B, Scialom G, Vautard R (2005) SIRTA, a ground-based atmospheric observatory for cloud and aerosol research. Ann Geophys 23:253–275

Hagelberg CR, Gamage NKK (1994) Structure-preserving wavelet decompositions of intermittent turbulence. Boundary-Layer Meteorol. 70:217–246

Howell JF, Mahrt L (1994) An adaptive decomposition: application to turbulence. In: Foufoula-Georgiou E, Kumar P (eds) Wavelets in geophysics. Academic Press, San Diego, pp 107–128

Kaimal JC, Finnigan JJ (1994) Atmospheric boundary layer flows – their structure and measurement. Oxford University Press, Oxford, 289 pp

Kanda M, Hino M (1993) Organized structures in developing turbulent flow within and above a plant canopy, using a large eddy simulation. Boundary-Layer Meteorol 68:237–257

Katul G, Kuhn G, Schieldge J, Hsieh C (1997) The ejection-sweep character of scalar fluxes in the unstable surface layer. Boundary-Layer Meteorol 83:1–26

Krusche N, De Oliveira AP (2004) Characterization of coherent structures in the atmospheric surface layer, Boundary-Layer Meteorol 110:191–211

Lee X, Neumann HH, Den Hartog G, Fuentes JD, Black TA, Mickle RE, Yang PC, Blanken PD (1997) Observation of gravity waves in a boreal forest. Boundary-Layer Meteorol 84:383–398

Lu C-H, Fitzjarrald DR (1994) Seasonal and diurnal variations of coherent structures over a deciduous forest. Boundary-Layer Meteorol 69:43–69

McNaughton KG, Brunet Y (2002) Townsend's hypothesis, coherent structures and Monin-Obukhov similarity. Boundary-Layer Meteorol 102:161–175

Nieuwstadt FTM (1984) The turbulent structure of the stable, nocturnal boundary layer. J Atmos Sci 41:2202–2216

Paw U KT, Brunet Y, Collineau S, Shaw RH, Maitani T, Qiu J, Hipps L (1992) On coherent structures in turbulence above and within agricultural plant canopies. Agric For Meteorol 61:55–68

Poulos GS, Burns SP (2003) An evaluation of bulk Ri-based surface flux formulas for stable and very stable conditions with intermittent turbulence. J Atmos Sci 60:2523–2537

Qiu J, PawU KT, Shaw RH (1995) Pseudo-wavelet analysis of turbulence patterns in three vegetation layers. Boundary-Layer Meteorol 72:177–204

Raupach MR, Finnigan JJ, Brunet Y (1996) Coherent eddies and turbulence in vegetation canopies: the mixing-layer analogy. Boundary-Layer Meteorol 78:351–382

Raupach MR, Thom AS, Edwards I (1980) A wind-tunnel study of turbulent flow close to regularly arrayed rough surfaces. Boundary-Layer Meteorol 18:373–397

Robinson SK (1991) Coherent motions in the turbulent boundary layer. Ann Rev Fluid Mech 23:601–639

Sadani LK, Kulkarni JR (2001) A study of coherent structures in the atmospheric surface layer over short and tall grass. Boundary-Layer Meteorol 99:317–334

Schols JLJ (1984) The detection and measurement of turbulent structures in the atmospheric surface layer. Boundary-Layer Meteorol 29:39–58

Stull R (1988) An introduction to boundary layer meteorology. Kluwer Academic Publishers, Dordrecht, 666 pp

Su H-B, Shaw RH, Paw U KT, Moeng C-H, Sullivan PS (1998) Turbulent statistics of neutrally stratified flow within and above a sparse forest from large-eddy simulation and field observations. Boundary-Layer Meteorol 88:363–397

Thomas C, Foken T (2006) Organised motion in a tall spruce canopy: temporal scales, structure spacing and terrain effects. Boundary-Layer Meteorol. doi:10.1007/s10546-006-9087-z

Torrence C, Compo GP (1998) A practical guide to wavelet analysis. Bull Amer Meteor Soc 79:61–78

Turner BJ, Leclerc MY, Gauthier M, Moore KE, Fitzjarrald DR (1994) Identification of turbulence structures above a forest canopy using a wavelet transform. J Geophys Res 99:1919–1926

Wallace JM, Eckelmann H, Brodkey RS (1972) The wall region in turbulent shear flow. J Fluid Mech 54:39–48

Wilczak JM (1984) Large-scale eddies in the unstably stratified atmospheric surface layer Part I: velocity and temperature structure. J Atmos Sci 41:3537–3550